Waveform inversion

Waveform inversion (WI) represents a family of techniques for velocity model building using seismic wavefields (Tarantola, 1984; Woodward, 1992; Pratt, 1999; Sirgue and Pratt, 2004; Plessix, 2006; Vigh and Starr, 2008; Plessix, 2009; Symes, 2009). This type of methodology, although usually regarded as one of the costliest techniques for velocity estimation, has been gaining momentum in recent years, mainly due to its accuracy and to advances in computing technology.

A key component of WI is wavefield simulation using a wave-equation, typically an acoustic wave-equation. Usually, WI is implemented in the data-domain, by adjusting the velocity model such that simulated and recorded data match. This match is based on the strong assumption that the wave-equation used for simulation is consistent with the earth – unlikely to be the case when the earth is characterized by strong (poro)elastic effects. Significant effort is often directed toward removing the components of the recorded data that are inconsistent with the assumptions used. Another key component of WI is the objective function (OF) used to measure the match between the simulated and recorded data. It is assumed that the OF is more-or-less convex, which allows for its minimization using gradient-based techniques. Thus, successful implementation of WI requires an effective (i.e. quick and robust) implementation of the gradient of the objective function.

An effective gradient calculation is based on the adjoint state method (Plessix, 2006; Symes, 2009). In summary, this method consists of the following steps: (1) compute the *state variables*, i.e. the seismic wavefields obtained from the source by forward modeling; (2) compute the *adjoint source*, i.e. a calculation based on the OF and on the state variables; (3) compute the *adjoint state variables*, i.e. the seismic wavefields obtained from the adjoint source by backward modeling; (4) compute the *gradient* using the state and adjoint state variables.

It is generally understood that WI should be implemented in the data-domain. Here, we show that WI can be similarly implemented in the image-domain, as suggested by Symes (2009). We show that the two implementations are not different in their use of seismic wavefields, but merely in their implementation of the OF gradient when multiple seismic experiments (e.g. shots) are considered. We present a comparative derivation of the data-domain and image-domain implementations and illustrate the less common image-domain method with a synthetic example.

Data-domain gradient

The state variables for the adjoint state method are obtained by solving the acoustic wave-equation

$$\mathcal{L}\left(\mathbf{x},\omega,m\right)u_s\left(\mathbf{e},\mathbf{x},\omega\right)=f_s\left(\mathbf{e},\mathbf{x},\omega\right)\ , \tag{1}$$

where $\mathcal{L}$ denotes the wave operator, u_s is the simulated wavefield, f_s is the source data, m are the model parameters (velocity or slowness), $\mathbf{e}$ is the experiment index, ω is the frequency, and $\mathbf{x}$ are the space coordinates $\{x,y,z\}$. A similar discussion can be done using a time-domain implementation, but we omit that here, for simplicity.

Conventional WI is an inverse problem with the model found by minimizing an OF defined using the difference between the observed and simulated wavefields, u_o and u_s (Tarantola, 1984; Pratt, 1999):

$$\mathcal{H}=\sum_{\mathbf{e}}\frac{1}{2}\|K_D\left(\mathbf{e},\mathbf{x}\right)\left(u_s\left(\mathbf{e},\mathbf{x},\omega\right)-u_o\left(\mathbf{e},\mathbf{x},\omega\right)\right)\|^2_{\mathbf{x},\omega}\ . \tag{2}$$

Here, K_D is a mask operator which limits the definition of the OF to specific locations, e.g. to positions on the surface. This common objective function suffers, among other things, from cycle skipping due to the oscillatory nature of the subtracted wavefields. This problem is usually addressed by bootstrapping the frequency from low to high (Sirgue and Pratt, 2004).

An alternative OF uses the correlation of the observed and simulated wavefields, instead of their difference (van Leeuwen and Mulder, 2010):

$$\mathcal{H}_D=\sum_{\mathbf{e}}\frac{1}{2}\|K_D\left(\mathbf{e},\mathbf{x}\right)P\left(\tau\right)c\left(\mathbf{e},\mathbf{x},\tau\right)\|^2_{\mathbf{x},\tau}\ , \tag{3}$$

where c is the correlation between the observed and simulated wavefields:

$$c\left(\mathbf{e},\mathbf{x},\tau\right)=\sum_{\omega}u_s\left(\mathbf{e},\mathbf{x},\omega\right)\overline{u_o\left(\mathbf{e},\mathbf{x},\omega\right)}e^{2i\omega\tau}\ , \tag{4}$$

and τ is the cross-correlation time-lag. The overline indicates complex conjugation, and P is an operator penalizing correlation energy outside zero time-lag. This operator is similar to the differential semblance optimization (DSO) penalty of Shen and Symes (2008).

We obtain the gradient of the OF ($\mathcal{H}$) using the adjoint state-method (Plessix, 2006; Symes, 2009): first we compute the adjoint source as the derivative of the OF relative to the state variables u_s:

$$g_s\left(\mathbf{e},\mathbf{x},\omega\right)=\frac{\partial\mathcal{H}_D}{\partial u_s}=K_D\left(\mathbf{e},\mathbf{x}\right)\overline{K_D\left(\mathbf{e},\mathbf{x}\right)}\sum_{\tau}P\left(\tau\right)\overline{P\left(\tau\right)}\Re\left(c\left(\mathbf{e},\mathbf{x},\tau\right)u_o\left(\mathbf{e},\mathbf{x},\omega\right)e^{-2i\omega\tau}\right)\ , \tag{5}$$

where $\Re$ takes the real part of the complex wavefields; then we compute the adjoint state variable a_s as a wavefield simulated backward in time using the adjoint source:

$$\mathcal{L}^{*}\left(\mathbf{x},\omega,m\right)a_s\left(\mathbf{e},\mathbf{x},\omega\right)=g_s\left(\mathbf{e},\mathbf{x},\omega\right)\ , \tag{6}$$

where the * sign indicates that the receiver wavefield is constructed by the operator $\mathcal{L}$ backward in time; finally we compute the constrained gradient of the OF using the correlation between the state and adjoint state variables, u_s and a_s:

$$\frac{\partial\mathcal{A}_D}{\partial m}\left(\mathbf{x}\right)=\sum_{\mathbf{e}}\sum_{\omega}\omega^2\overline{u_s\left(\mathbf{e},\mathbf{x},\omega\right)}a_s\left(\mathbf{e},\mathbf{x},\omega\right)\ , \tag{7}$$

where $\mathcal{A}_D$ is the constrained (augmented) OF (Plessix, 2006).

Image-domain gradient

A similar procedure can be implemented in the image-domain with extended images obtained by wave-equation migration (downward continuation or reverse-time), using the time-lag imaging condition (Sava and Fomel, 2006; Sava and Vasconcelos, 2011). The state variables are represented by the source and receiver wavefields, u_s and u_r, simulated using the source wavelet f_s and the recorded data f_r:

$$\begin{bmatrix}\mathcal{L}\left(\mathbf{x},\omega,m\right) & 0\\ 0 & \mathcal{L}^{*}\left(\mathbf{x},\omega,m\right)\end{bmatrix}\begin{bmatrix}u_s\left(\mathbf{e},\mathbf{x},\omega\right)\\ u_r\left(\mathbf{e},\mathbf{x},\omega\right)\end{bmatrix}=\begin{bmatrix}f_s\left(\mathbf{e},\mathbf{x},\omega\right)\\ f_r\left(\mathbf{e},\mathbf{x},\omega\right)\end{bmatrix}\ . \tag{8}$$

The wavefields u_s and u_r are obtained by forward and backward modeling, respectively. In this case, we can formulate the OF as

$$\mathcal{H}_I=\frac{1}{2}\|K_I\left(\mathbf{x}\right)P\left(\tau\right)r\left(\mathbf{x},\tau\right)\|^2_{\mathbf{x},\tau}\ , \tag{9}$$

where r is the time-lag extended image (Sava and Fomel, 2006)

$$r\left(\mathbf{x},\tau\right)=\sum_{\mathbf{e}}\sum_{\omega}\overline{u_s\left(\mathbf{e},\mathbf{x},\omega\right)}u_r\left(\mathbf{e},\mathbf{x},\omega\right)e^{2i\omega\tau}\ , \tag{10}$$

and K_I is a mask operator which restricts the evaluation of the OF to some locations in the image. The penalty operator P is identical to the operator used in the data-domain. Then, we compute the gradient of the OF by defining an adjoint sources

$$\begin{bmatrix}g_s\left(\mathbf{e},\mathbf{x},\omega\right)\\ g_r\left(\mathbf{e},\mathbf{x},\omega\right)\end{bmatrix}=\begin{bmatrix}\frac{\partial\mathcal{H}_I}{\partial u_s}\\ \frac{\partial\mathcal{H}_I}{\partial u_r}\end{bmatrix}=\begin{bmatrix}K_I\left(\mathbf{x}\right)\overline{K_I\left(\mathbf{x}\right)}\sum_{\tau}P\left(\tau\right)\overline{P\left(\tau\right)}\Re\left(r\left(\mathbf{x},\tau\right)\overline{u_r\left(\mathbf{e},\mathbf{x},\omega\right)}e^{-2i\omega\tau}\right)\\ K_I\left(\mathbf{x}\right)\overline{K_I\left(\mathbf{x}\right)}\sum_{\tau}P\left(\tau\right)\overline{P\left(\tau\right)}\Re\left(r\left(\mathbf{x},\tau\right)u_s\left(\mathbf{e},\mathbf{x},\omega\right)e^{-2i\omega\tau}\right)\end{bmatrix}\ , \tag{11}$$

computing the adjoint state variables, a_s (backward modeling) and a_r (forward modeling),

$$\begin{bmatrix}\mathcal{L}^{*}\left(\mathbf{x},\omega,m\right) & 0\\ 0 & \mathcal{L}\left(\mathbf{x},\omega,m\right)\end{bmatrix}\begin{bmatrix}a_s\left(\mathbf{e},\mathbf{x},\omega\right)\\ a_r\left(\mathbf{e},\mathbf{x},\omega\right)\end{bmatrix}=\begin{bmatrix}g_s\left(\mathbf{e},\mathbf{x},\omega\right)\\ g_r\left(\mathbf{e},\mathbf{x},\omega\right)\end{bmatrix}\ , \tag{12}$$

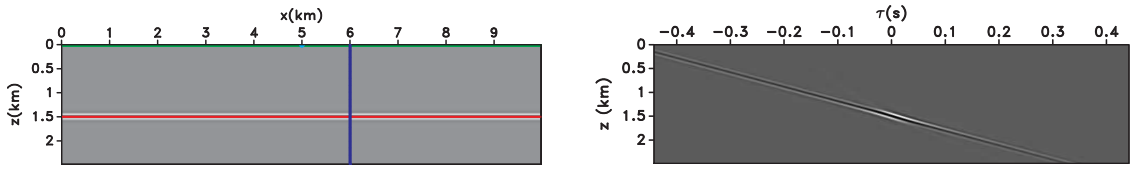

(a) (b)

Figure 1: (a) Conventional image and (b) extended image in the time-lag domain obtained with the correct velocity after summation over all shots distributed throughout the surface. The red line indicates the exact position of the reflector. The maximum energy in the time-lag gather is located at $\tau = 0$ and at the correct reflector depth, $z = 1.5$ km.

and evaluating the gradient by the correlation of the state (u_s, u_r) and adjoint state variables (a_s, a_r)

$$\frac{\partial \mathcal{A}_I}{\partial m}(\mathbf{x}) = \sum_{\mathbf{e}} \sum_{\omega} \omega^2 \left(\overline{u_s(\mathbf{e},\mathbf{x},\omega)} a_s(\mathbf{e},\mathbf{x},\omega) + \overline{u_r(\mathbf{e},\mathbf{x},\omega)} a_r(\mathbf{e},\mathbf{x},\omega) \right) , \tag{13}$$

where $\mathcal{A}_I$ is the constrained (augmented) OF (Plessix, 2006).

Example

We illustrate the method with a simple synthetic model. We restrict our attention to the image-domain implementation. The model consists of a horizontal reflector in constant velocity. Figure 1(a) shows the image obtained by migration using the correct velocity, and Figure 1(b) shows the time-lag gather obtained at $x = 6$ km after summation over all shots located on the surface. Figures 2(a)-2(c)-2(e)-2(g) depict the image, the extended image, the adjoint source and the gradient of the OF for a slow background velocity, and Figures 2(b)-2(d)-2(f)-2(h) depict the equivalent objects for a high background velocity. We can observe the familiar band-limited wavepaths with opposite signs, according to the velocity anomalies. This gradient corresponds to one shot located at $x = 5$ km, and similar wavepaths could be obtained from any other locations in the image for all other shots. The total gradient is then obtained by summation over all shots (experiments). Here we consider a common-image-gather at a fixed surface position, although a similar result is possible with sparse common-image-point-gathers (Sava and Vasconcelos, 2011).

Conclusions

WI can be formulated both in the data-domain or in the image-domain. The OF can be formulated using wavefield correlations instead of differences, thus eliminating the need for (very) low frequency in the data which are required to reduce cycle skipping. The same wavefields are used in both cases (i.e. the same wave-equation, the same sources and boundary conditions, etc), therefore these implementations are not at all different from this point of view. The data-domain OF applies a time-lag penalty to the correlation of the simulated and observed wavefields before summation over experiments. This OF uses correlations only on the surface at the known locations of the receivers. In contrast, the image-domain OF applies a time-lag penalty to the correlation of the source and receiver wavefields after summation over experiments, i.e. it exploits the semblance principle. This OF uses correlations at any locations in the image, including surface locations. This technique works for any type of seismic experiment (point source, plane source, etc) and the wavefield reconstruction can be implemented equally well in the time-domain or in the frequency-domain. No cumbersome time-lag picking is necessary to define the image-domain objective function.

Acknowledgments

We acknowledge the sponsors of the Center for Wave Phenomena at Colorado School of Mines. The reproducible numeric examples use the Madagascar open-source package (http://www.reproducibility.org).

REFERENCES

Plessix, R.-E., 2006, A review of the adjoint state method for computing the gradient of a functional with geophysical applications: Geophysical Journal International, **167**, 495–503.

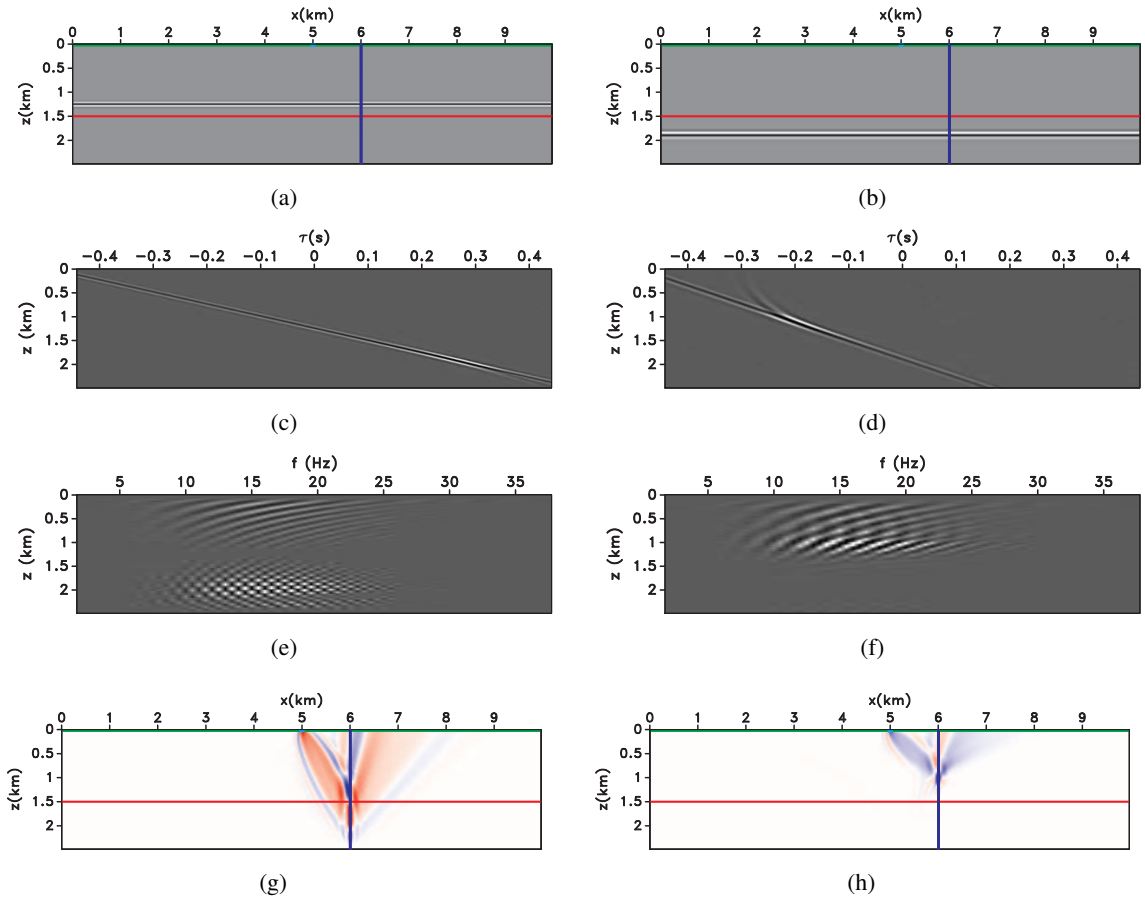

Figure 2: The panels depict from top to bottom the conventional image, extended image, frequency-domain adjoint source and OF gradient. The left and right columns correspond to low and high velocities, respectively.

———, 2009, Three-dimensional frequency-domain full-waveform inversion with an iterative solver: Geophysics, **74**, WCC53–WCC61.

Pratt, R. G., 1999, Seismic waveform inversion in the frequency domain, Part 1: Theory and verification in a physical scale model: Geophysics, **64**, 888–901.

Sava, P., and S. Fomel, 2006, Time-shift imaging condition in seismic migration: Geophysics, **71**, S209–S217.

Sava, P., and I. Vasconcelos, 2011, Extended imaging condition for wave-equation migration: Geophysical Prospecting, **59**, 35–55.

Shen, P., and W. W. Symes, 2008, Automatic velocity analysis via shot profile migration: Geophysics, **73**, VE49–VE59.

Sirgue, L., and R. Pratt, 2004, Efficient waveform inversion and imaging: A strategy for selecting temporal frequencies: Geophysics, **69**, 231–248.

Symes, W., 2009, Migration velocity analysis and waveform inversion: Geophysical Prospecting, **56**, 765–790.

Tarantola, A., 1984, Inversion of seismic reflection data in the acoustic approximation: Geophysics, **49**, 1259–1266.

van Leeuwen, T., and W. A. Mulder, 2010, A correlation-based misfit criterion for wave-equation traveltime tomography: Geophysical Journal International, **182**, 1383–1394.

Vigh, D., and E. W. Starr, 2008, 3D prestack plane-wave, full-waveform inversion: Geophysics, **73**, VE135–VE144.

Woodward, M. J., 1992, Wave-equation tomography: Geophysics, **57**, 15–26.